Distribution of reaction strength in ^{32}S + ^{182}W collisions

J. G. Keller, B. B. Back, B. G. Glagola, D. Henderson, S. B. Kaufman, S. J. Sanders,
R. H. Siemssen,* F. Videbaek, B. D. Wilkins, and A. Worsham†
Argonne National Laboratory, Argonne, Illinois 60439
(Received 27 April 1987)

The reaction ^{32}S + ^{182}W has been studied at beam energies of 166, 177, 222, and 260 MeV with the goal of accounting for the distribution of the total reaction cross section among the main reaction channels. Cross sections as well as mass and energy distributions were measured over the entire angular range from 10° to 170° for elastic (which includes quasi-elastic), deep-inelastic, and fission-like products. Deep inelastic scattering accounts for a substantial fraction of the total reaction cross section at all energies, in particular near the barrier. This behavior is not predicted by current theories such as the extra push model. The angular distributions of fission-like products are more anisotropic than expected on the basis of the saddle point model at the two lowest energies, indicating a sizable contribution from quasi-fission processes, which is estimated from a quantitative analysis of this deviation.

I. INTRODUCTION

Studies of the interaction between heavy ion projectiles and heavy target nuclei have proven very useful in developing an understanding of the dynamics of nuclear matter at low energies. Investigation of the fission process was for decades the only means of studying properties such as the mass rearrangement, energy dissipation arising from shape changes, and the underlying shape dependent potential energy surface. With the discovery of the deep-inelastic scattering process, two new important aspects of nuclear dynamics were brought into play, namely the time scale and large angular momenta, both of which are associated with the angular velocity of the system. More recently, the discovery of quasi-fission processes provides the link between the deep-inelastic scattering processes, for which the energy dissipation is the main aspect, and the compound fission processes, where the dissipation of energy is complete. With the quasi-fission process, we have the opportunity to study the nuclear dynamics in terms of the interplay between reaction time, energy dissipation, and angular momentum, as well as the relations to the complete fusion-fission and deep-inelastic scattering processes. The term quasi-fission refers to fully damped processes with a substantial net mass transfer between the two interacting nuclei. Such processes are distinct from complete fusion-fission processes by failing to produce a completely fused system inside the fission barrier.

Recently, theoretical[1-5] models have become available which describe the competition between the different damped reaction channels, i.e., deep-inelastic, quasi-fission, and complete fusion processes, in a quantitative manner. These models are based on classical trajectory calculations including Coulomb, nuclear, centrifugal, and dissipative terms, the latter of which, in most cases, is based on the one-body dissipation mechanism.

Although rather extensive comparisons with experimental data have been made,[6-11] these have concentrated mainly on capture or complete fusion processes, where capture refers to the sum of complete fusion and quasi-fission processes. It is the hope, however, that systematic experimental studies of the division of the reaction strength between the various reaction channels, i.e., quasi-elastic, deep-inelastic, quasi-fission, and complete fusion, will help provide a more detailed understanding of heavy-ion reactions at energies near the interaction barrier and lead to a refinement of the theoretical models describing such processes.

The division of reaction strength, as well as the energy dissipation and mass asymmetry relaxation properties for the ^{32}S + ^{182}W system, are in the present experiment studied as a function of the bombarding energy. We have measured the deep-inelastic component in addition to the capture processes, and compared the relative contributions to model predictions. We find that the deep-inelastic component contributes a surprisingly large fraction of the total cross section for damped reactions at energies near the interaction barrier. This behavior is not predicted for such a light system and it calls for a reconsideration of the basic assumption of the present theories.

In the present work we have studied the properties of the fission-like components in detail. The measured angular distributions are compared to the predictions of the saddle point model. At the lower energies, it is found that the measured anisotropies are higher than expected on the basis of this model. This deviation is interpreted as a clear signature for a significant quasi-fission component, the strength of which is estimated from a quantitative comparison with the theory. At the two higher beam energies, a large fraction of the fission-like cross section is associated with spin values larger than those which can be supported by the ^{214}Th compound system, i.e., the fission barrier vanishes. This fraction of the fission-like cross section must necessarily come from quasi-fission processes. This conclusion is supported by the fact that a weak, but possibly

significant, forward-backward asymmetry is observed in the average mass of fission-like products at the two highest beam energies. This asymmetry is incompatible with fission decay from a completely fused system with a lifetime longer than the rotational period of the system (of the order $\tau \simeq 10^{-20}$ s).

The description of the experimental procedure is presented in Sec. II followed by a discussion of the corrections for the detector response and the data analysis in Sec. III. The discussion of the differential and angular integrated cross sections for the different reaction channels is presented in Sec. IV, whereas the distributions with respect to fragment mass and total kinetic energy of the fission-like products are presented in Sec. V, followed by a summary.

II. EXPERIMENTAL SETUP

The experiment was performed in the 165 cm diameter scattering chamber at the Argonne superconducting linac (ATLAS). The tightly collimated ^{32}S beam was focused on a target of 100 μg/cm^2 ^{182}W evaporated onto a 20 μg/cm^2 carbon backing. The target material was facing upstream in order to allow the low energy fragments emitted into the backward hemisphere to emerge without suffering energy loss in the backing material. Reaction products and elastically scattered particles were detected in eight, low resistivity Si surface-barrier fission detectors operated in a singles mode and positioned at angles between 10° and 170° (Fig. 1). An additional Si detector was used to monitor elastic scattering at 20° for cross-section normalization. The fission detectors had active areas of 400 mm^2 and were 60 μm thick. All Si detectors measured energy as well as the time of flight of the detected particles relative to the time structure of the beam, which had a repetition rate of 12.125 MHz. The binary nature of the reaction kinematics was checked by placing a two-dimensional, position sensitive, parallel-plate avalanche counter (PPAC) of 80×100 mm^2 on the opposite side of the beam axis in order to register coincident reaction partners. All detectors were positioned at distances between 400 and 600 mm from the target.
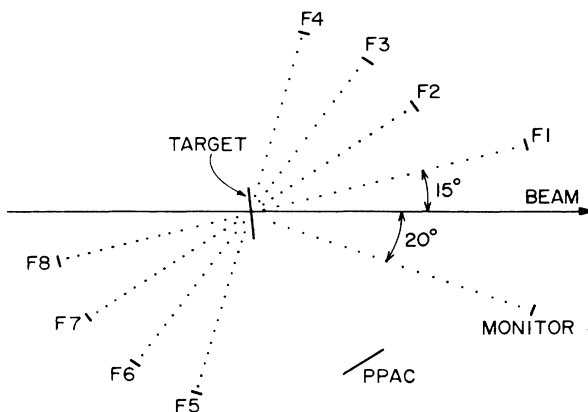

FIG. 1. Illustration of the experimental setup.

The precision of the time-of-flight measurement was determined chiefly by the beam structure. An overall time resolution of approximately $\Delta t \sim 350$ ps was achieved. The energy resolution for elastically scattered S ions was typically $\Delta E \simeq 2$–3 MeV, which results in a mass resolution for projectile-like fragments of $\Delta A \simeq 2$ u. It is estimated that the typical mass resolution for fission-like fragments is somewhat poorer, probably around $\Delta A \simeq 5$ u, because of a less accurate detector response and a larger energy straggling in the target for these heavier and slower moving ions. The natural widths of the mass and energy distributions of fission-like fragments are, however, typically an order of magnitude larger than the detector resolution, hence, the results are quite insensitive to the detector resolution as long as adequate corrections for the centroid shifts caused by these detector shortcomings are applied. We shall discuss these corrections in detail in the following section.

III. DATA ANALYSIS

The data analysis was carried out by reconstructing the primary reaction kinematics event by event. Corrections for the pulse height defect and the plasma delay (associated with the measurement of heavy ions in Si detectors) were applied in order to obtain the correct energy and mass of the final fragments. In order to deduce the kinematic properties of the primary reaction, assumed to be of binary nature, it is furthermore necessary to correct for energy losses in the target material and sequential emission of post-fission neutrons from the primary, highly excited fragments.

A. Calibration

The absolute energy calibration of the Si detectors was determined from elastic scattering data at all beam energies, correcting for the pulse height defect and the energy loss in the target material. The size of the pulse height defect was, for each detector, determined on the basis of the pulse height spectrum of fission fragments from a ^{252}Cf source according to the procedure proposed by Kaufman et al.[12]

The time dispersions were determined from the beam pulse separation of 82.5 ns. The time offsets were determined from the position of the elastic scattering peak in the time spectrum and the known flight time of elastically scattered beam particles from the target to the detector. Although the timing of the elastically scattered particles, with respect to the radio frequency of the accelerator, varied with beam energy, the relative time calibration for each detector was independent of beam energy. The time offsets of all detectors relative to the monitor detector were determined at the lowest beam energy of 166 MeV where elastically scattered particles were observed in all detectors. The time offset of the monitor detector was determined from elastic scattering at each beam energy.

B. Event-by-event analysis

In the event-by-event reconstruction of the reaction kinematics, several experimental limitations had to be taken into account. The observed energy signal was corrected for the pulse height defect assumed to depend on energy and mass of the detected particle as given by Kaufman *et al.*[12] For symmetric fission fragments this correction amounts to 3–10 % of the measured signal.

The time signal of surface barrier detectors for heavy ions is delayed with respect to the track formation by space-charge effects.[13] Although, in principle, this delay is both energy and mass dependent, a linear mass dependence was assumed in the present analysis with the elastically scattered sulfur ions and the corresponding recoils used to determine this dependence. The effect of correcting the mass versus kinetic energy spectra for the plasma delay is illustrated in Fig. 2.

The energy losses of beam particles and reaction products in the target and backing material were calculated according to the prescription of Braune and Schwalm.[14] A correction for this energy loss was applied to obtain the initial energy of the fragment before emerging from the target.
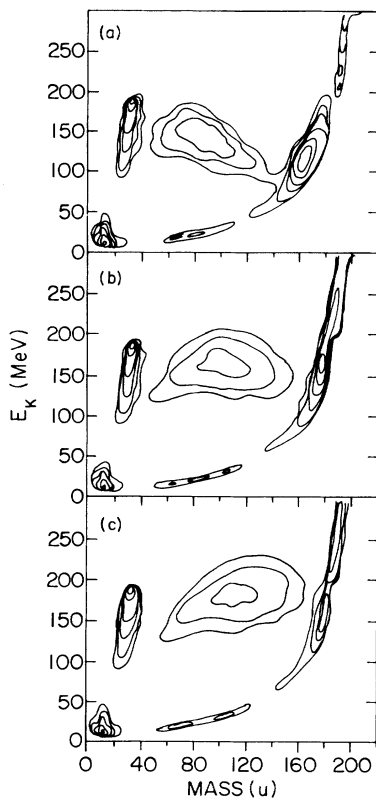

FIG. 2. Illustration of the sensitivity to the plasma delay correction for the data taken at $\theta_{c.m.} \simeq 90°$ and $E_{lab} = 222$ MeV. The effect of applying no correction [panel (c)], the calibrated correction [panel (b)], and twice the calibrated plasma delay correction is shown as contour plots for the count rate vs fragment mass and total kinetic energy. Contour lines are shown for $\sigma = 0.01, 0.03, 0.1, 0.3, 1,$ and 3 mb/sr/u.

The masses of reaction products were also corrected for post-fission neutron evaporation in order to obtain the primary mass and energy distributions. The number of neutrons emitted from the detected fragment was estimated on the basis of the final fragment mass, the associated excitation energy and neutron binding energy of the primary fragment. The excitation energy was calculated from the ground state Q value and the total kinetic energy release for the specific mass division. The Q values and neutron binding energies necessary for this calculation are averaged over the five isotones centered at the Z corresponding to a uniform charge distribution between the two fragments. The excitation energy was divided between the two fragments according to their mass corresponding to a constant temperature for the system. The average kinetic energy of the neutrons was taken as proportional to the temperature, i.e., $E_n = 2T$.

C. Systematic errors in energy and time measurement

The experimental accuracy of the derived mass and total energy distributions arise from the systematic errors in the energy and time measurements. The accuracy of the computed mass depends primarily on the accuracy of the corrections for the plasma delay to the time measurement and the pulse height defect correction to the energy measurement. The plasma delay correction for a symmetric fission fragment is of the order $\Delta t \simeq 1.5$ ns. By adjusting the magnitude of this correction to reproduce the correct masses for elastically scattered ^{32}S ions and recoiling ^{182}W ions, an adjustment which also leads to the average fission fragment mass of $A_{sym} = 107$ u at $\theta_{c.m.} \simeq 90°$ as required, we estimate that the systematic error on the time measurement is less than 20% of the size of the correction, i.e., $\delta t \simeq 0.3$ ns.

The systematic error associated with the energy measurement arises mainly from the uncertainty in the pulse height defect correction, which assumed a typical value of $\Delta E \simeq 8$ MeV for symmetric fission fragments. We estimate that this correction is applied with an accuracy of about $\delta E \simeq 0.8$ MeV. Additional systematic errors are associated with the energy loss in the target foil and the correction for neutron evaporation from the primary fragments. Each of these corrections is estimated to be associated with a systematic error of $\delta E \simeq 0.6$ MeV, which results in a total systematic error on the primary fragment energy of $\delta E \simeq 1.2$ MeV.

Propagating the systematic errors on the time and energy measurements results in overall systematic errors of $\delta A \simeq 2.5$ u and $\delta E_K \simeq 5$ MeV on the primary fragment mass and the total kinetic energy release for symmetric fission. These systematic errors are generally larger than any statistical errors, the contribution of which is ignored in the present analysis.

The systematic errors on the widths of the mass and total energy distributions are of the order of $\delta(\sigma_A) \simeq 0.3$ u and $\delta(\sigma E_K) \simeq 0.8$ MeV. The statistical errors on these quantities combined with the errors associated with the operational division between fission and deep-inelastic scattering are typically larger than the systematical errors arising from the energy and time measurements.

We have therefore assigned the larger statistical errors to these quantities.

D. Check for binary kinematics

To calculate kinematics it was assumed that all processes observed can be treated as binary reactions. This assumption was tested by examining the folding angle distribution of coincident fragments in one of the surface barrier detectors and the PPAC counter. The average folding angle agrees with the expectations based on total fission kinetic energies taken from the Viola systematics,[15] both at 166 and 260 MeV beam energy. Although the accuracy of this measurement is insufficient to exclude a small contribution of incomplete fusion processes, such processes are expected to play a rather insignificant role at the beam energies of the present experiment. Furthermore, any contribution of sequential fission processes, i.e., fission of the target-like reaction partner after a quasi-elastic or deep-inelastic primary reaction is expected to be negligible because of the relatively high fission barrier of the target-like nuclei.

IV. CROSS SECTIONS

The decomposition of the total reaction cross section into its individual components may be observed directly in Fig. 2(b). Elastic and quasi-elastic scattering of the ^{32}S beam gives rise to an intense peak at $A \simeq 32$ u and $E_K \simeq 189$ MeV with a tail of deep inelastic scattering processes toward lower kinetic energies. Fission-like fragments (from complete fusion-fission and quasi-fission processes) account for the wide distribution in the center of the figure. The heavy reaction partners from quasi-elastic and deep-inelastic processes appear as a curved disjoint band which extends from the upper right-hand corner of the figure down to $A \simeq 50$ u and $E_K \simeq 10$ MeV. The masses for the low energy tail of this distribution are severely underestimated because of inadequate detector response for very low energy heavy fragments. Reaction products from the carbon and oxygen impurities in the target are seen in the lower left-hand corner of the figure.

The cross section for evaporation residues is expected to be negligibly small and is not observed in the present experiment. Extrapolating from measurements[16] on the systems ^{216,218,220}Th produced in complete fusion of ^{40}Ar and ^{176,178,180}Hf, it is expected that the total evaporation residue cross section is of the order $\sigma_{ER} \simeq 1-10$ μb over the excitation energy range of the present data.

A. Elastic scattering — total reaction cross section

The energy and mass resolution in this experiment was insufficient to distinguish between elastic scattering, inelastic excitation, and transfer processes. All processes with an energy dissipation of up to 8–15 MeV are therefore included in the elastic plus quasi-elastic scattering yield. The ratio of this elastic plus quasi-elastic scattering cross section to the Rutherford cross section is shown as solid points in Fig. 3. The data were normalized to the monitor detector, which was positioned at an
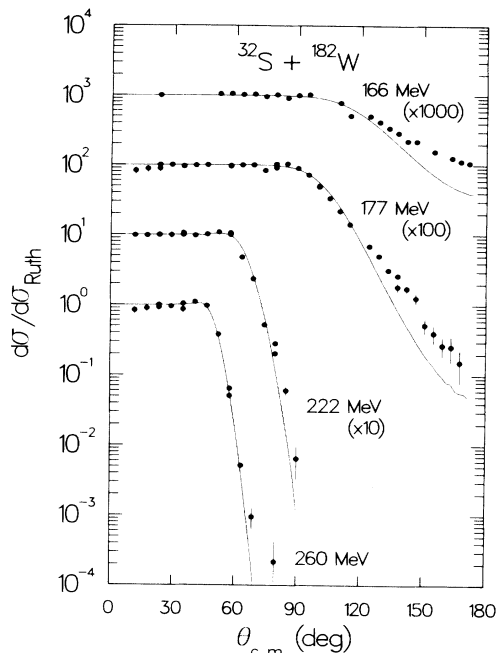

FIG. 3. Ratio of elastic plus quasi-elastic scattering and Rutherford cross section for four beam energies. Solid curves are obtained from optical model calculations (see text).

angle ($\theta_{lab} = 20°$) of pure Rutherford scattering.

The total cross section for damped reactions, "σ_{reac}", was determined experimentally by the sum-of-differences method[17] according to which

$$\text{``}\sigma_{reac}\text{''} = 2\pi \int_{\theta_{gr}}^{\pi} \sin\theta \, \sigma_{Ruth}(\theta)$$

$$\times \left[1 - \frac{\sigma_{el}(\theta) + \sigma_{qe}(\theta)}{\sigma_{Ruth}(\theta)} \right] d\theta . \quad (1)$$

The total reaction cross sections obtained in this manner are listed in Table I.

Optical model calculations, using the code PTOLEMY,[18] were also carried out in an attempt to reproduce the measured angular distributions. The results of such calculations, using an energy independent potential defined by $V = W = 40$ MeV, $r = 1.168$ fm, $r' = 1.242$ fm, and $a = a' = 0.5$ fm, are shown as solid curves in Fig. 3. The cross sections obtained from these calculations agree, within errors, with the ones extracted directly from the data using the above procedure.

B. Angular distribution for deep-inelastic scattering

Deep-inelastic (DI) processes were distinguished from quasi-elastic scattering by their greater energy dissipation (events with energy losses larger than 8–15 MeV were counted as DI events) and from fission fragments by their mass — all fragments with masses below 40 mass units were considered to originate from scattering processes. The separation between quasi-elastic and deep-inelastic processes is the main source of error in deter-

TABLE I. Angle integrated cross sections

E_{lab} (MeV)	"σ_{reac}"[b] (mb)	$\sigma_{\text{DI}}+\sigma_{\text{fis}}$ (mb)	σ_{DI} (mb)	σ_{fis}[c] (mb)	σ_{CF}[d] (mb)
166	365±30	355±65	175±65	180±20	25±25
177	680±50	630±70	210±55	420±45	320±100
222	1550±100	1375±125	430±75	945±100	565±150
260	1970±100	1830±220	605±160	1225±150	630±250
170[a]				240±25	105±90
180[a]				440±45	195±50
200[a]				700±70	
210[a]				700±80	415±110
220[a]				950±100	480±210
240[a]				1130±120	810±190

[a]Reanalysis of data taken from Ref. 21.
[b]Obtained by analysis of elastic plus quasi-elastic scattering cross sections, Sec. IV A.
[c]Cross section for fission-like processes, i.e., complete fusion-fission and quasi-fission.
[d]Obtained by analysis of the angular distributions of fission-like products.

mining the cross section for DI scattering. An illustration of the separation between these two processes is shown in Fig. 4. We observe that the deep-inelastic scattering yield extends down to the Viola[15] energy characteristic for the fission process. This corresponds to the Coulomb repulsion energy between two coaxial spheroids with a minor to major axis ratio of $b/a \simeq 0.6$ and a surface separation of $d \simeq 2$ fm.

A Wilczynski plot of the scattering cross section as a function of angle and kinetic energy is shown in Fig. 5. At angles smaller than $\theta_{\text{lab}} \simeq 30°$ it was not possible to distinguish between DI scattering, slit scattering, and evaporation residues of ^{32}S with oxygen or carbon in the target. Hence, only data at larger angles are included in the angular distributions, which are shown as solid points in Fig. 6. Smooth solid curves are drawn through

the data points on the basis of which the angle integrated cross sections are obtained; these are listed in Table I. The estimated uncertainty includes the error associated with extrapolating to more forward angles as illustrated by dashed curves. This extrapolation takes into account the possibility of an undetected forward peaked component of the angular distribution.

C. Angular distribution of fission-like fragments

In the present data, fission-like fragments are well separated from scattering processes. Only at small angles ($< 20°$) relative to the target plane is the separation of fission products from elastic recoils problematic due to substantial energy-loss straggling in the target. Fragments with very low energies ($E_{\text{frag}} < 10$ MeV) could not
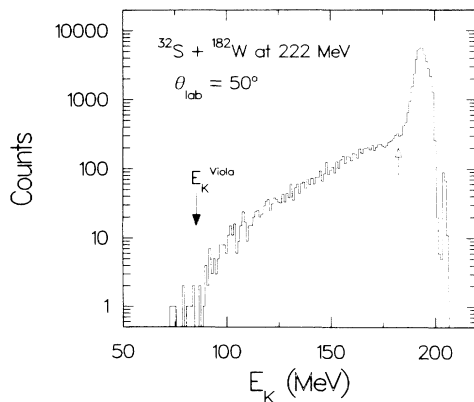

FIG. 4. Example for the distinction between quasi-elastic and deep-inelastic scattering. The open arrow indicates the point of separation between the two reaction types. The solid arrow indicates the energy expected on the basis of the Viola systematics (Ref. 15). Products with masses $A < 40$ u are included in this spectrum.
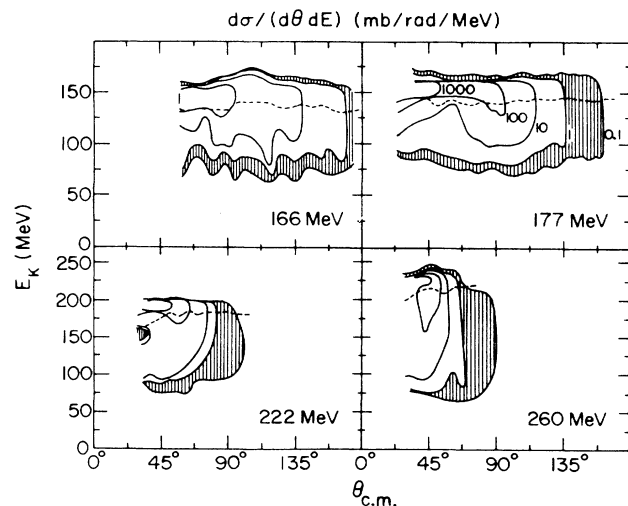

FIG. 5. Wilczynski plot of the scattering cross section as function of center-of-mass angle and total kinetic energy for four beam energies. The dashed lines represent the division between deep-inelastic and quasi-elastic scattering.
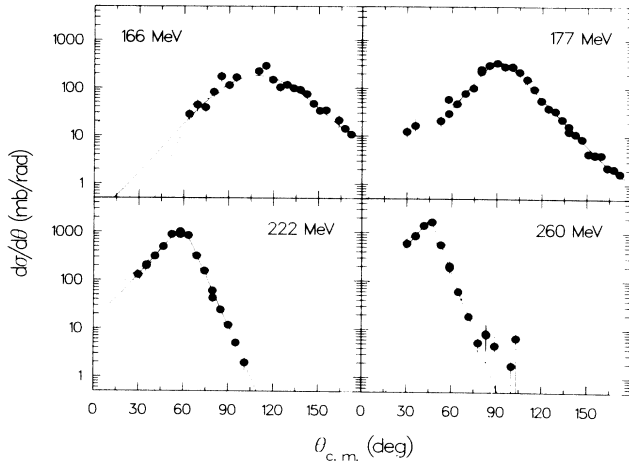
FIG. 6. Measured deep-inelastic cross sections $(d\sigma/d\theta)$ as a function of angle for four energies. The solid curves represent the optimum fits to the data, dashed curves indicate the range of possible extrapolations beyond the measured angular range.

be detected and fragments with energies close to the energy of elastically scattered projectiles were at small scattering angles sometimes indistinguishable from slit scattering. The energy and mass distributions were corrected for these losses but large uncertainties at the most forward and backward angles are associated with the inaccuracy of these corrections. In general, the uncertainty was estimated to be 50% of the correction. The statistical uncertainties, also included, are mostly negligible. The measured angular distributions are shown as solid points in Fig. 7 .
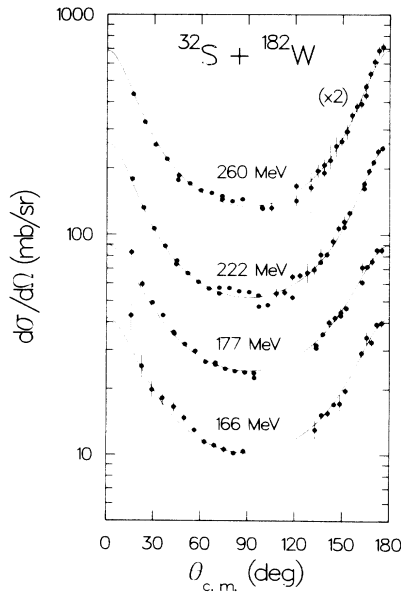

FIG. 7. Angular distributions for fission-like products. Solid curves represent the best fits to the data.

The angular distribution for compound nucleus fission may be written

$$W(\theta)= \sum_{I=0}^{\infty} (2I+1)P(I)$$

$$\times \sum_{K=-I}^{I} \tfrac{1}{2}(2I+1)\rho(K,I)\,|\,d_{0,K}^{I}(\theta)\,|^{2}\,, \qquad (2)$$

which involves a summation over the spin I and its projection K on the symmetry axis of the fissioning system. In this formula, $d_{M,K}^{I}(\theta)$ is the symmetric top wave function and $P(I)$ the fusion probability for the partial wave I. The fusion probabilities were obtained from a calculation which describes the measured excitation function. This calculation takes into account the effects of static and dynamic target deformations, which give rise to an enhanced subbarrier fusion cross section as well as substantial tails in the fusion probability function $P(I)$ for large spin values. The model used for this calculation is described in detail in Ref. 18. The parameters used were $\delta_2=0.50$, $\sigma_2=0.020$, $\sigma_0=2.0$. If the final distribution of K values, $\rho(K,I)$, reflects a statistical equilibrium at a particular stage in the process (e.g., the saddle point), one obtains the following expression on the basis of simple level density arguments:[20]

$$\rho(K,I)= \exp(-K^{2}/2K_0^{2}) \left[\sum_{K=-I}^{I} \exp(-K^{2}/2K_0^{2}) \right]^{-1},$$

$$(3)$$

where

$$K_0^2= \frac{J_{\rm eff}}{\hbar^2} T_{\rm sad}, \quad \frac{1}{J_{\rm eff}}=\frac{1}{J_\|}-\frac{1}{J_\perp}\,. \qquad (4)$$

In this expression

$$T_{\rm sad}=[\,8.5(E^{*}-B_f-E_{\rm rot})/A\,]^{1/2}$$

is the nuclear temperature at the saddle point, where E^* is the excitation energy of the compound system, B_f is the fission barrier, and $E_{\rm rot}$ is the rotational energy. The moments of inertia parallel and perpendicular to the nuclear symmetry axis at the saddle point of the fissioning system are denoted $J_\|$ and $J_\perp$ respectively.

The full drawn curves of Fig. 7 are calculated on the basis of Eq. (3) by varying K_0^2 to obtain the best fit to the data. The resulting values of K_0^2 are listed in Table II and plotted as solid points in Fig. 8 as a function of the mean square spin of the fissioning system. Open circles are obtained from a reanalysis of an earlier set of data.[21]

The experimental estimates of K_0^2 are compared with theoretical predictions based on the saddle point shapes predicted by the rotating liquid drop model[22] (solid curve) as well as the finite range model[23] (dashed curve). It is evident that the K_0^2 values obtained from the analysis of the angular distribution data are systematically lower than both of these theoretical estimates. This effect has been observed for a large number of reactions involving heavy projectiles, and interpreted as a consequence of quasi-fission processes contributing to the cross section of fission-like products. The present

TABLE II. Parameters relevant for the analysis of the angular distribution of fission-like fragments. The nuclear temperature T_{sad} relates to the fission saddle point, $\langle I^2 \rangle$ is the mean square spin of the fissioning system and J_0 is the rigid moment of inertia for a spherical compound system. For further details see Refs. 9 and 10.

E_{lab} (MeV)	T_{sad} (MeV)	$\langle I^2 \rangle$ ($\hbar^2$)	K_0^2 ($\hbar^2$)	J_0/J_{eff}
166	1.42	1350	88±24	1.51±0.41
177	1.50	1850	144±32	0.97±0.22
222	1.83	4235	206±49	0.79±0.19
260	2.07	6065	288±107	0.61±0.23
170[a]	1.44	1575	118±42	1.14±0.40
180[a]	1.55	1945	110±25	1.51±0.23
200[a]	1.72	2915	111±32	1.41±0.40
210[a]	1.76	3380	186±33	0.85±0.16
220[a]	1.83	4125	196±70	0.82±0.30
240[a]	1.92	5360	312±77	0.53±0.14

[a]Reanalysis of data taken from Ref. 21.

data are in good agreement with the empirical systematics on the occurrence of this process. These systematics also reflect the general trends predicted by the extra-extra push model—although there are differences in the details.[11]

For comparison, we also show the K_0^2 values to be expected, if a statistical equilibrium in the appropriate degree of freedom (tilting) were established at the scission point[9,24] (dashed-dotted curve in Fig. 8). We see that the present data fall in between the predictions of the saddle and the scission point models indicating that the K_0^2 distribution may be frozen in somewhere between these two points.
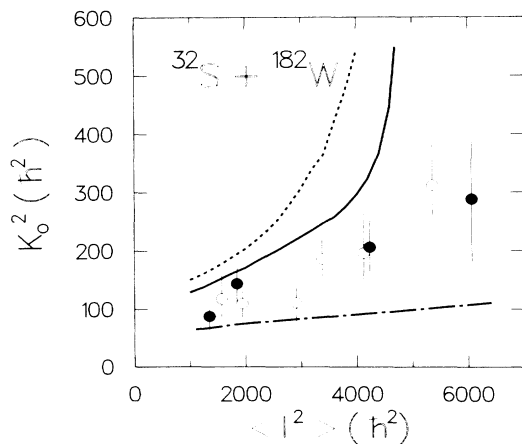

FIG. 8. Experimental values of K_0^2 (solid points, present data; open points, Ref. 19) are shown as a function of the average mean square spin and compared to predictions of the rotating liquid drop model (solid curve), the finite range model (dashed curve), and the scission point model (dash-dotted curve).

D. Estimate of complete fusion and quasi-fission cross sections

An estimate of the contribution of quasi-fission processes to the fission-like cross section may be obtained from a quantitative analysis of the observed angular anisotropy. This method of analysis has been applied successfully to a wide body of fission angular distribution data and is described in more detail in Ref. 9. It is based on the assumption that the quasi-fission component is associated with the highest partial waves, whereas fission of compound nuclei formed in complete fusion reactions originate from the low partial waves. It is furthermore assumed that the anisotropy of this latter component is well described by the saddle point model and that the angular distribution for the quasi-fission component is given by an effective moment of inertia of $J_0/J_{eff} = 1.5$. The separation between complete fusion-fission and quasi-fission processes is assumed to occur at a well defined spin, which is determined from fitting the measured angular distributions. Although this assumption clearly is too simplistic, it is expected that using a more realistic smooth transition between complete fusion and quasi-fission processes will not significantly affect the derived cross sections.

Estimates of the complete fusion cross sections σ_{CF}, obtained in such an analysis, are shown as triangles in Fig. 9 and listed in Table I. We observe that this analysis leads to a substantial contribution of quasi-fission reactions, which is the difference between the capture and complete fusion cross sections. In the following subsection, we discuss this division of the total reaction cross section in more detail.

E. Energy dependence of angle-integrated cross sections

In Fig. 9, we summarize the division of the damped reaction strength between the various reaction channels. The total cross section for damped reactions may be estimated either as the sum (solid squares) of its individual components, (deep-inelastic scattering and fission-like processes) or as the integrated difference (open diamonds) between the observed elastic plus quasi-elastic scattering cross section and Rutherford scattering behind the grazing angle as described in Sec. IV A. Both estimates of the reaction cross sections are compared to optical model calculations (dotted curve), using the potential listed in Sec. IV A.

The angle integrated cross sections for fission-like processes are represented by solid (present work) and open circles (Ref. 9). These are compared with the cross sections for capture reactions (dashed curve) as predicted by the extra-extra push model using the parameters obtained by Shen *et al.*[25] These parameters are $x_{th} = 0.62$, $a = 7.3$, $f = 0.55$, and $\mu = 0.37$. We find that the capture cross section, calculated in this manner, are in good agreement with the measured cross sections for fission-like processes. Furthermore, we find that the complete fusion-fission cross sections, represented by closed and open triangles, agree well with the corresponding predictions (solid curve) from the extra-extra push model.
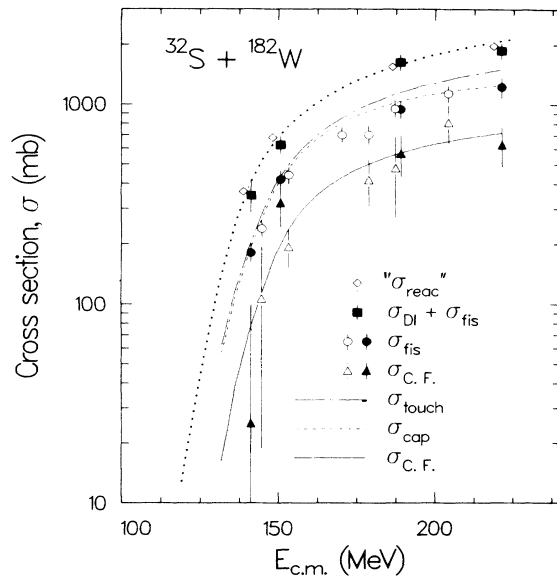
FIG. 9. Angle integrated cross sections as a function of center-of-mass energy. Total cross sections for damped reactions (open diamonds), fission-like plus deep inelastic cross sections (solid squares), fission-like cross sections [solid and open (Ref. 21) circles], and complete fusion cross sections [solid and open (Ref. 21) triangles] are shown. The results of optical model calculations for the total reaction cross section are represented by the dotted curve whereas the predictions for touching, capture and complete fusion reactions by the extra-extra push model are shown as dashed-dotted, dashed, and solid curves, respectively.

A large discrepancy between the extra-extra push model calculations and the experimental results is present for the cross section for deep-inelastic scattering. In the calculation, this cross section is represented by the difference between the cross section, σ_{touch}, for traversing the interaction barrier (dashed-dotted curve in Fig. 9), and the cross section for capture behind the conditional saddle point, σ_{cap}. The calculations predict only very small cross sections for deep-inelastic processes, whereas large cross sections ranging from $\sigma_{DI} = 175-605$ mb are observed experimentally. This observation clearly represents a challenge for the theoretical model, possibly suggesting that the majority of deep-inelastic processes, in this case, are associated with trajectories outside the interaction barrier.

In comparisons with calculations at the two highest beam energies, based on the macroscopic model of Feldmeier,[26] we find that large energy losses are associated with trajectories, which do not traverse the interaction barrier. This effect gives rise to deep-inelastic cross sections compatible with the ones observed experimentally. At beam energies closer to the barrier, this model fails to account for the observed cross sections, mainly because it does not include the effects of fluctuations in the barrier height. It is well known[27,28] that such effects give rise to a large enhancement of the capture cross section at near barrier energies. Consequently we cannot expect the model to apply in this energy range.

V. MASS AND TOTAL KINETIC ENERGY DISTRIBUTIONS

Contour diagrams of the cross sections $(d\sigma/d\Omega)$ with respect to fragment mass and total kinetic energy for the three highest beam energies at 90° in the center-of-mass system are shown in Fig. 10. The dashed curves represent the mass dependence of the total kinetic energy expected for pure Coulomb repulsion between two fragments with a quadrupole deformation compatible with the Viola energy at mass symmetry.[15] We note that the deep-inelastic component extends from the elastic energies of $E_K(\text{el}) = 150$, 189, and 221 MeV, respectively, down to the completely damped energy of $E_K \simeq 90-100$ MeV at all three beam energies. The fission-like fragments are clearly separated from the scattering products at all energies. The total kinetic energies obtained from the measurement of the elastic and deep-inelastic recoil products are associated with large uncertainties because of their low kinetic energies in the laboratory system.

A. Mass distributions

In systems where quasi-fission is the dominating process it has been found[7,10,25,29] that there is often a distinct angle dependence of the mean fragment mass (forward-backward asymmetry), a feature which is incompatible with compound nucleus fission. This
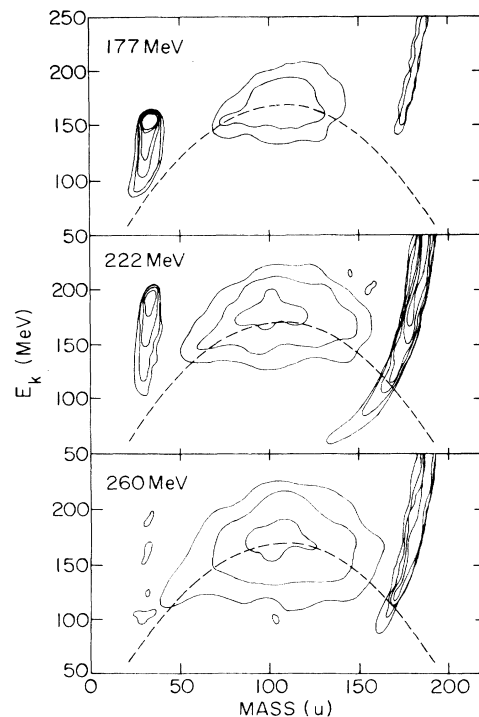

FIG. 10. Contour diagrams of the cross section as a function fragment mass and total kinetic energy are shown for three beam energies at $\theta_{c.m.} = 90°$. Contour lines are shown for $\sigma = 0.01$, 0.03, 0.1, 0.3, 1, and 3 mb/sr/u. The dashed curves represent Coulomb repulsion energies between two deformed fragments.

forward-backward asymmetry arises because the reaction time is comparable with the rotational period of the system.

The present data show only very weak angular dependence of the average mass (Fig. 11). At the two lower energies ($E_{beam} = 166$ and 177 MeV) the average mass is angle independent, whereas at the higher energies there appears to be a slight angle dependence with heavier masses being emitted preferentially at forward angles. It is not certain, however, that this effect is significant in view of the systematic errors associated with the various corrections described in Sec. II. Assuming that this deviation is indeed significant it would support the conclusion from the analysis of the angular distributions that there is a component of quasi-fission in the observed fission-like cross section. It should be noted, however, that the absence of a forward-backward asymmetry does not exclude the presence of a quasi-fission component since observation of asymmetry relies solely on the reaction time being comparable to the rotational period of the system. If, for instance, the reaction time for the quasi-fission process is substantially longer than the rotational period, this signature would be lost.

The width of the mass distribution, expressed in terms of the standard deviation σ_A, is found to be independent of angle at all beam energies. It does, however, increase slowly with beam energy, or equivalently, the excitation energy of the fissioning system (Fig. 12). The numerical values of σ_A are listed in Table III.

The increase in the mass width as a function of excitation energy is consistent with the statistical model treatment of the mass asymmetry degree of freedom as shown by the dashed curve in Fig. 12(a). If the mass asymmetry potential at the scission point is approximated by a parabolic shape with a force constant k, we find

$$\sigma_A^2 = \frac{T_{scis}}{k} , \tag{5}$$

where T_{scis} is the nuclear temperature at the scission point;

$$T_{scis} = [8.5(E^* + Q_{sym} - E_K - E_{def} - E_{rot})/A]^{1/2} , \tag{6}$$

where Q_{sym} is the reaction Q value for symmetric mass split, E_{def} is the energy bound in fragment deformation estimated at ~ 12 MeV from studies of low energy fission in the actinide region, $E_{c.m.}$ is the center-of-mass energy of the reaction, E_{rot} is the rotational energy of the complex, and E_K is the Viola[15] estimate of the total kinetic energy, which is identified with the Coulomb repulsion energy at scission. We have adjusted the value of k to reproduce the mass widths observed for the two lower energies $E = 166$ and 177 MeV which results in a value of $k = 0.0060$ MeV/u^2. This is in good agreement with the value of k obtained for the neighboring system ^{40}Ar + ^{176}Hf → ^{216}Th (Ref. 30) ($k = 0.0061$ MeV/u^2). At the higher beam energies σ_A is underestimated (Fig. 12), possibly indicating that the observed mass distribution is not solely determined by a statistical equilibrium at the scission point. Instead, the fission-like fragments associated with the higher partial waves most likely have their origin in quasi-fission processes, where the mass asymmetry is not completely equilibrated with other degrees of freedom of the system. Similar deviations from the
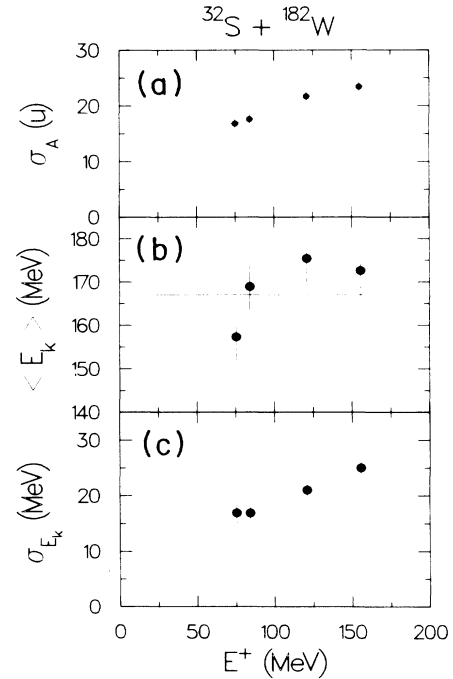
FIG. 12. The standard deviations σ_A of the fragment mass distributions, are shown [panel (a)] as a function of excitation energy at the saddle point. The dashed curve is the result of a theoretical calculation adjusted to the two lowest points. The average total kinetic energy, $\langle E_K \rangle$ [panel (b)], and the associated standard deviation, σ_E [panel (c)], are shown as a function of the excitation energy at the scission point, E^+. The horizontal line in the upper plot represents the prediction from the Viola systematics (Ref. 15).
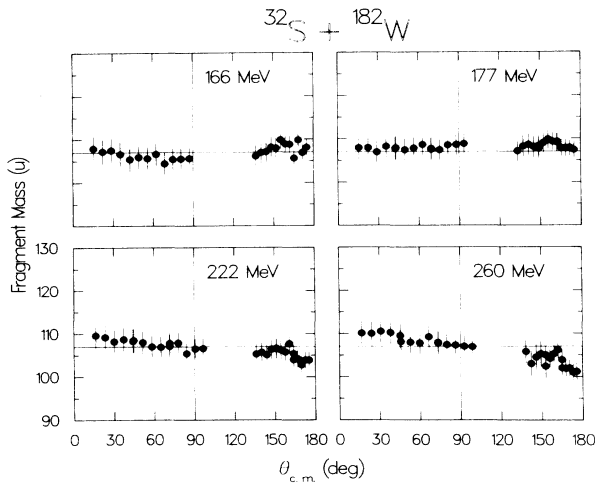

FIG. 11. The average mass of fission-like products is shown as a function of the scattering angle at beam energies of 166, 177, 220, and 260 MeV.

TABLE III. Parameters relevant to the fragment mass and total kinetic energy distributions at $\theta_{c.m.} = 90°$. T_{scis} is the nuclear temperature at the scission point, $\langle A_{frag} \rangle$ and σ_A the centroid and standard deviation of the fragment mass distribution, respectively, whereas $\langle E_K \rangle$ and σ_E are the corresponding quantities for the total kinetic energy distribution.

E_{lab} (MeV)	T_{scis} (MeV)	$\langle A_{frag} \rangle$ (u)	σ_A (u)	$\langle E_K \rangle$ (MeV)	σ_E (MeV)
166	1.72	105±2	16.8±1.0	162±5	18.6±1.0
177	1.83	109±2	17.6±1.0	169±5	17.9±1.0
222	2.19	107±2	21.7±1.0	177±5	20.9±1.0
260	2.48	107±2	23.4±1.0	171±5	25.1±1.0

statistical behavior have been observed in heavier systems[25] where a quasi-fission contribution clearly is present.

B. Total kinetic energy distributions

Within experimental errors, which are rather large as a result of measuring only one of the two final fragments in the reaction, the average total kinetic energy, $\langle E_K \rangle$, is independent of the scattering angle. This behavior is expected for both fission and quasi-fission reactions, both of which are characterized by a complete relaxation of the kinetic energy. The total kinetic energy arises chiefly from the Coulomb repulsion between the fragments at the scission point, reflecting the shape of the system at this point.

In Fig. 12 we show the dependence of the total kinetic energy release and its standard deviation, σ_E, as a function of the excitation energy at the scission point,

$$E^+ = E_{c.m.} + Q_{sym} - E_K - E_{def},$$

where $E_{c.m.}$ is the center-of-mass energy, Q_{sym} is the reaction Q value for symmetric mass division, and E_{def} is the deformation energy of the fragments taken to be $E_{def} = 12$ MeV. The total kinetic energy is compared to the Viola systematics[15] as represented by a horizontal line. We observe a reasonable agreement with this empirical systematics. The rather large systematic errors associated with this quantity do, however, preclude a study of a possible increase in total kinetic energy with mean angular momentum as observed for the ^{32}S+Sm reaction.[31]

The standard deviation of the total kinetic energy, σ_E, is seen to increase smoothly with excitation energy at the scission point. This behavior is expected for a statistical equilibrium, since an increase in temperature allows for a wider distribution in phase space and consequently kinetic energy release. We have, however, not attempted to perform a more quantitative comparison with theory on account of the relatively poor quality of the total kinetic energy measurement.

VI. SUMMARY

In the present study we have measured the cross sections for elastic and deep-inelastic scattering as well as fission-like processes over the angular range $\theta_{lab} = 10°-170°$ for beam energies of $E_{lab} = 166$, 177, 222,

and 260 MeV. The angular distributions for fission-like processes are analyzed on the basis of the saddle point model of fission. Angular anisotropies larger than expected on the basis of this model are interpreted in terms of the presence of a quasi-fission component, the size of which is derived from a quantitative analysis of the discrepancy. The sum of cross sections for deep-inelastic scattering and fission-like processes is compared with the total cross section for damped reactions obtained from an analysis of the angular distributions for elastic plus quasi-elastic scattering, and we find consistency between these two independent ways of obtaining the total reaction cross section.

The angle integrated cross sections for complete fusion, quasi-fission, and deep-inelastic processes are compared to calculations with the extra-extra push model, the parameters of which have been determined from a previous analysis of a large set of data for complete fusion and capture reactions, mostly for heavier reaction systems. We find that the model describes both the complete fusion and quasi-fission cross sections quite well, but fails to account for the substantial cross section observed for deep-inelastic scattering processes at each of the four beam energies. This discrepancy may arise from the assumption that deep-inelastic scattering processes are associated only with trajectories which proceed inside the interaction barrier. Indeed, it appears that energy losses of the magnitude normally attributed to deep-inelastic scattering processes may result also for trajectories, which remain outside the interaction barrier. Such trajectories are found in calculations based on the dynamical model of Feldmeier.[26] The calculations show that at the point of closest approach the system is in sufficiently close contact to form a small neck between the two reaction partners. The subsequent deformation of the fragments and the energy dissipation in the separation phase of the reaction gives rise to the large energy losses, which places such trajectories in the category of deep-inelastic scattering processes. On the other hand, it is not impossible that part of the discrepancy arises from a somewhat arbitrary division between quasi-elastic and deep-inelastic processes either experimentally, theoretically or both. More detailed calculations and a comparison with the experimental Q-value spectra would, however, be able to resolve these questions.

Special emphasis was placed on the measurement of fragment masses in order to look for an angle dependence as a clear signal for a component of quasi-fission

processes. Although the determination of fragment masses is associated with several experimental uncertainties arising from the properties of solid-state Si detectors, we have been able to correct for these defects and obtain reliable mass distributions, at least in the forward hemisphere. We find that the average mass for fission-like products is independent of scattering angle for the two lowest beam energies as expected for the fission decay after complete fusion. At the two higher energies there is an indication that heavy fragments are preferentially emitted in the forward hemisphere, although this deviation is only marginally significant. It should, however, be kept in mind that approximate equality between the reaction time and the rotational period is required for this signal to be present. Thus, there may well be a substantial quasi-fission contribution, as indicated by the fragment angular distributions, without this manifesting itself in the mass-angle distributions.

In conclusion we find a surprisingly strong contribution of deep-inelastic processes and indications of a significant component of quasi-fission processes, although these do not give rise to a strong angle dependence of the fragment mass distributions. This latter observation probably indicates that the associated reaction times are relatively long compared to the rotational period.

ACKNOWLEDGMENTS

*On leave from Kernfysisch Versneller Instituut der Rijksuniversiteit, Groningen, The Netherlands.

†Present address: Yale University, New Haven, CT 06511.

[1] W. J. Swiatecki, Phys. Scr. **24**, 113 (1981); Nucl. Phys. **A376**, 275 (1982).

[2] S. Bjørnholm and W. J. Swiatecki, Nucl. Phys. **A391**, 471 (1982).

[3] R. Donangelo and L. F. Canto, Nucl. Phys. **A453**, 349 (1986).

[4] J. P. Błocki, H. Feldmeier, and W. J. Swiatecki, Gesellschaft für Schwerionenforschung (Darmstadt) (GSI) Report No. GSI-86-16, 1986.

[5] J. R. Nix and A. J. Sierk, in Proceedings of the International School-Seminar on Heavy Ion Physics, Dubna, USSR, 1986.

[6] M. Blann and D. Akers, Phys. Rev. C **26**, 465 (1982).

[7] R. Bock, Y. T. Chu, M. Dakowski, A. Gobbi, A. Olmi, H. Sann, D. Schwalm, U. Lynen, W. F. J. Müller, S. Bjørnholm, H. Esbensen, W. Wölfli, and E. Morenzoni, Nucl. Phys. **A388**, 334 (1982).

[8] J. Tõke, R. Bock, G. X. Dai, A. Gobbi, S. Gralla, K. D. Hildenbrand, J. Kuzminski, W. F. J. Müller, A. Olmi, W. Reisdorf, S. Bjørnholm, and B. B. Back, Phys. Lett. **142B**, 258 (1984).

[9] B. B. Back, Phys. Rev. C **31**, 2104 (1985); **32**, 1786 (1985).

[10] J. Tõke, R. Bock, G. X. Dai, S. Gralla, A. Gobbi, K. D. Hildenbrand, J. Kuzminski, W. F. J. Müller, A. Olmi, H. Stelzer, B. B. Back, and S. Bjørnholm, Nucl. Phys. **A440**, 327 (1985).

[11] W. Q. Shen, J. Albinski, A. Gobbi, S. Gralla, K. D. Hildenbrand, N. Herrmann, J. Kuzminski, W. F. J. Müller, H. Stelzer, J. Tõke, B. B. Back, S. Bjørnholm, and S. P. Sørensen, Phys. Rev. C **36**, 115 (1987).

[12] S. B. Kaufman, E. P. Steinberg, B. D. Wilkins, J. Unik, A. J. Gorski, and M. J. Fluss, Nucl. Instrum. Methods **115**, 47 (1974).

[13] W. Bohne, W. Galster, K. Grabisch, and H. Morgenstern, Nucl. Instrum. Methods A **240**, 145 (1985).

[14] K. Braune, D. Schwalm, GSI Annual Report GSI-J-1-77, 1977, p. 177.

[15] V. E. Viola, Jr., Nucl. Data, Sect. **A1**, 391 (1966); V. E. Viola, K. Kwiatkowski, and M. Walker, Phys. Rev. C **31**, 1550 (1985).

[16] D. Vermeulen, H.-G. Clerc, C.-C. Sahm, K.-H. Schmidt, J. G. Keller, G. Münzenberg, and W. Reisdorf, Z. Phys. A **318**, 157 (1984).

[17] H. Oeschler, H. L. Harney, D. L. Hillis, and K. S. Sim, Nucl. Phys. **A325**, 463 (1979).

[18] M. H. Macfarlane, S. C. Pieper, Argonne National Laboratory (unpublished information); M. J. Rhodes-Brown, S. C. Pieper, and M. H. Macfarlane, Phys. Rev. C **21**, 2417 (1980).

[19] B. B. Back, R. R. Betts, J. E. Gindler, B. D. Wilkins, S. Saini, M. B. Tsang, C. K. Gelbke, W. G. Lynch, M. A. McMahan, and P. A. Baisden, Phys. Rev. C **32**, 195 (1985).

[20] I. Halpern and V. M. Strutinski, in *Proceedings of the Second UN International Conference on the Peaceful Uses of Atomic Energy, Geneva, Switzerland, 1957* (United Nations, Geneva, Switzerland, 1958), p. 408.

[21] B. Glagola *et al.*, Bull. Am. Phys. Soc. **26**, 550 (1981).

[22] S. Cohen, F. Plasil, and W. J. Swiatecki, Ann. Phys. (N.Y.) **82**, 557 (1974).

[23] A. J. Sierk, Phys. Rev. C **33**, 2039 (1986).

[24] P. D. Bond, Phys. Rev. C **32**, 421 (1985); **32**, 483 (1985).

[25] W. Q. Shen, J. Albinski, R. Bock, G. X. Dai, A. Gobbi, S. Gralla, K. D. Hildenbrand, N. Herrmann, J. Kuzminski, W. F. J. Müller, A. Olmi, H. Stelzer, J. Tõke, B. B. Back, S. Bjørnholm, S. P. Sørensen, A. Olmi, and G. Guarino, Europhys. Lett. **1**, 113 (1986).

[26] H. F. Feldmeier, Argonne National Laboratory Report ANL-PHY-85-2, 1985.

[27] C. Y. Wong, Phys. Rev. Lett. **31**, 766 (1973).

[28] H. Esbensen, Nucl. Phys. **A352**, 147 (1981).

[29] K. Lützenkirchen, J. V. Kratz, G. Wirth, W. Brüchle, K. Sümmerer, R. Lucas, J. Poitou, and C. Grégoire, Nucl. Phys. **A452**, 351 (1986).

[30] C.-C. Sahm, H. Schulte, D. Vermeulen, J. G. Keller, H.-G. Clerc, K.-H. Schmidt, F. P. Hessberger, and G. Münzenberg, Z. Phys. A **297**, 241 (1980).

[31] B. G. Glagola, B. B. Back, and R. R. Betts, Phys. Rev. C **29**, 486 (1984).